Cell Reports
Physical Science

CellPress
OPEN ACCESS

Article

Interfacial gliding-driven lattice oxygen release in layered cathodes

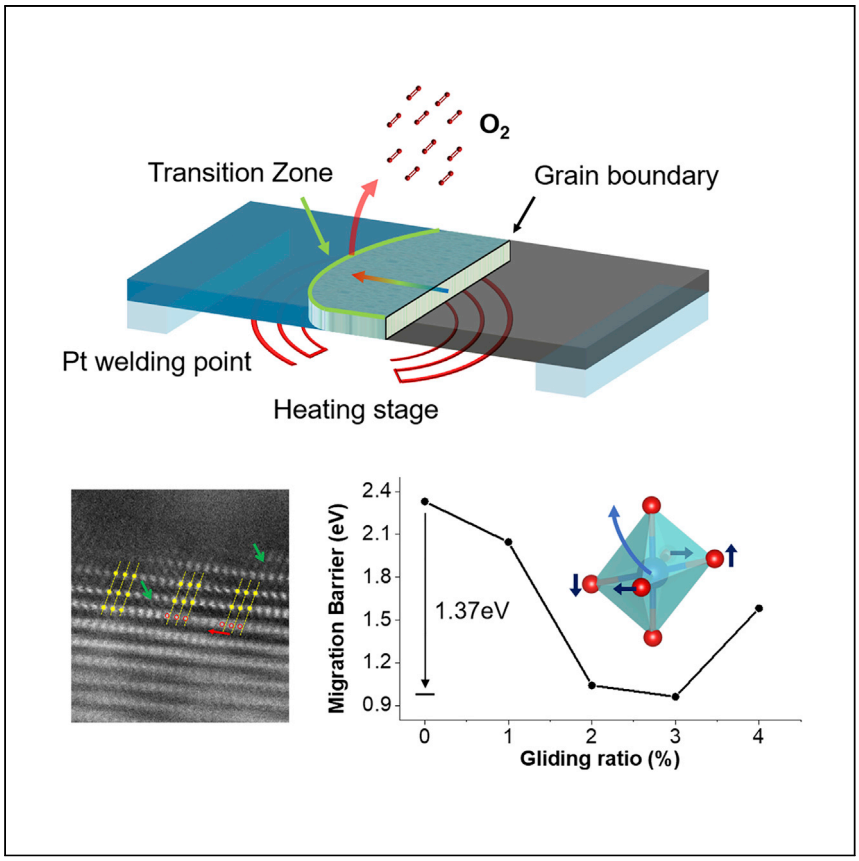

The release of the lattice oxygen is a critical issue in layered cathodes. Sun et al. report enhanced oxygen release susceptibility at the intergranular gliding, which originates from a significantly reduced octahedra trapping strength and could be mitigated by basal plane terminated low-angle boundary arrays.

Congli Sun, Xiaobin Liao, Haoyang Peng, Chenyu Zhang, Gustaaf Van Tendeloo, Yan Zhao, Jinsong Wu

yan2000@whut.edu.cn (Y.Z.)
wujs@whut.edu.cn (J.W.)

Highlights

Dynamic planar gliding at intergranular interfaces of layered cathodes

Enhanced local oxygen release susceptibility at the gliding initiation

Reduced cation trapping strength from the strain-coupled octahedra distortion

Sun et al., Cell Reports Physical Science 3, 100695
January 19, 2022
https://doi.org/10.1016/j.xcrp.2021.100695

Cell Reports
Physical Science

CellPress
OPEN ACCESS

Article

Interfacial gliding-driven lattice oxygen release in layered cathodes

Congli Sun,[1,2,5] Xiaobin Liao,[1] Haoyang Peng,[1,2] Chenyu Zhang,[3] Gustaaf Van Tendeloo,[2,4] Yan Zhao,[1,*] and Jinsong Wu[1,2,*]

SUMMARY

The oxygen release of layered cathodes causes many battery failures, but the underlying mechanism in an actual working cathode is still elusive as it involves secondary agglomerates that introduce complicated boundary structures. Here, we report a general structure instability on the mismatch boundaries driven by interfacial gliding—it introduces a shear stress causing a distortion of the metal-oxygen octahedra framework that reduces its kinetic stability. The migration of cations and diffusion of oxygen vacancies continue to degrade the whole particle from the boundary to the interior, followed by the formation of nano-sized cracks on the fast-degrading interfaces. This work reveals a robust chemical and mechanical interplay on the oxygen release inherent to the intergranular boundaries of layered cathodes. It also suggests that radially patterned columnar grains with low-angle planar boundaries would be an efficient approach to mitigate the boundary oxygen release.

INTRODUCTION

The release of the lattice oxygen is one of the most typical issues in layered lithium transition metal oxides (LTMO).[1,2] Oxygen release contributes to a number of battery failures, including the voltage/capacity fade,[3–6] loss of cation ions,[7] impedance rise,[8,9] cracking, and detachment of primary particles.[5,10–16] It also triggers thermal runaway events, raising a safety concern that is increasingly critical with the continuous capacity improvement toward high energy density.[17–24] Oxygen release has been widely investigated and is generally attributed to thermodynamically driven phase transitions that are intrinsic to layered cathodes.[17,21,23,25–29] Cathodes much easier lost oxygen under high-voltage cycling, at high states of charge, or with a high Ni content.[17,26,27,30–32] Most recent studies also revealed a strong facet anisotropy[20] and a significant kinetic stability due to cation migration barriers,[32,33] which explains well the surface/vacancy-dominated degradation, as well as general mitigating approaches such as facet/surface control, cation stabilization, and valence state homogenization. Exploring the origin of oxygen release clearly provides a fundamental basis for the rational design of stable cathodes.[1,4,5,7,10,32,34,35]

LTMO cathodes are usually secondary agglomerates comprising primary particles with complicated three-dimensional (3D) hierarchical structures.[10] The primary particles are densely packed with a large amount of intergranular boundaries, which leads to a high volumetric energy density with a mitigation of the side reactions from the cathode/electrolyte interface.[24] The intergranular boundary plays a critical role in the oxygen release issues, but the fundamental understanding of the

[1]State Key Laboratory of Advanced Technology for Materials Synthesis and Processing, International School of Materials Science and Engineering, Wuhan University of Technology, Wuhan 430070, China

[2]NRC (Nanostructure Research Centre), Wuhan University of Technology, Wuhan 430070, China

[3]School of Applied Engineering Physics, Cornell University, Ithaca, NY 14850, USA

[4]EMAT (Electron Microscopy for Materials Science), University of Antwerp, Antwerp, Belgium

[5]Lead contact

*Correspondence: yan2000@whut.edu.cn (Y.Z.), wujs@whut.edu.cn (J.W.)

https://doi.org/10.1016/j.xcrp.2021.100695

boundary contribution is still far from clear. One of the main challenges is the complex atomic arrangement at the boundary. Most intergranular boundaries are not optimized energetically, but rather formed kinetically with random grain orientations. This leads to innumerable high-energy boundaries with a significant interface reconstruction that is difficult to predict. Meanwhile, the incorporation of stress is severe at the boundary because of the anisotropic expansion/contraction. The coupling of the mechanical effect to the electrochemical performance is significant, but the fundamental mechanism remains unclear as the chemo-mechanical interplay is at the atomic level. This requires a high spatial and time resolution to achieve dynamic tracking of the stress and structure correlation. As such, the reported boundary contributions are often elusive and even controversial.

Here, *in situ* heating inside an aberration-corrected scanning transmission electron microscope (STEM) was performed to study the oxygen release along the intergranular boundaries of $LiCoO_2$, the prototype structure of LTMOs. A chip-based heating stage was used to achieve a high stability and reliability for the dynamic imaging. Interfacial gliding and shear stress was induced by the thermal expansion at high heating rates, which introduces locally a strong CoO_6 octahedra distortion along the intergranular boundaries that initiate the oxygen release. The diffusion of oxygen vacancies continues to drive an inward degradation that eventually affects the entire particle. Such a boundary oxygen release also features a strong surface effect for ion migration, as well as a significant crystallographic orientation dependence for a favorable ion and vacancy diffusion path. This study provides an atomic insight into a robust chemical and mechanical interplay on the oxygen release that generally exists on the highly mismatched intergranular boundaries of the layered cathodes. It also sheds light on the crystallographic design of layered cathodes with enhanced boundary oxygen ion stability.

RESULTS AND DISCUSSION

Heating rate-induced boundary degradation heterogeneity

Although both simulation and experiments exist in understanding the low-energy and coherent grain boundaries in LTMOs,[36–39] the intergranular boundary in an actual working cathode is formed by almost random orientations of primary particles with significant interface reconstructions, as shown in Figure S1 and Note S1. The reason is likely to be the limited rotation and translation freedom of the primary particles to obtain an energetically favorable attaching position during the synthesis. The lack of available facets to connect each primary grain could also be responsible. It is interesting that all of the intergranular boundaries are vulnerable at high heating rates, while in sharp contrast, boundaries are very stable at low heating rates, as shown in Figure 1. Figures 1A–1C are high-angle annular dark field (HAADF) STEM images of a secondary $LiCoO_2$ (LCO) particle at 550°C. The sample is heated with a heating rate of 50°C/s and remains at 550°C for imaging. It shows clear degradation starting from the intergranular boundaries, with a gradual propagation into the grain interiors. A completely different thermal behavior can be obtained at the same temperature of 550°C but at a much lower heating rate of 2°C/s. The heating is also paused at multiple intermediate temperatures before reaching 550°C to relax the thermal stress. As shown by the HAADF STEM images in Figures 1D–1F, the sample degrades at a much lower speed through the formation and growth of nanovoids; the degradation shows no clear sensitivity to the presence of the boundaries. A detailed nanovoid development with local phase dynamics was reported in our recent publication.[32] In fact, as long as the heating rate is slow enough, the boundary remains robust, even under severe phase degradation (Figure S2 and Note S2). Such

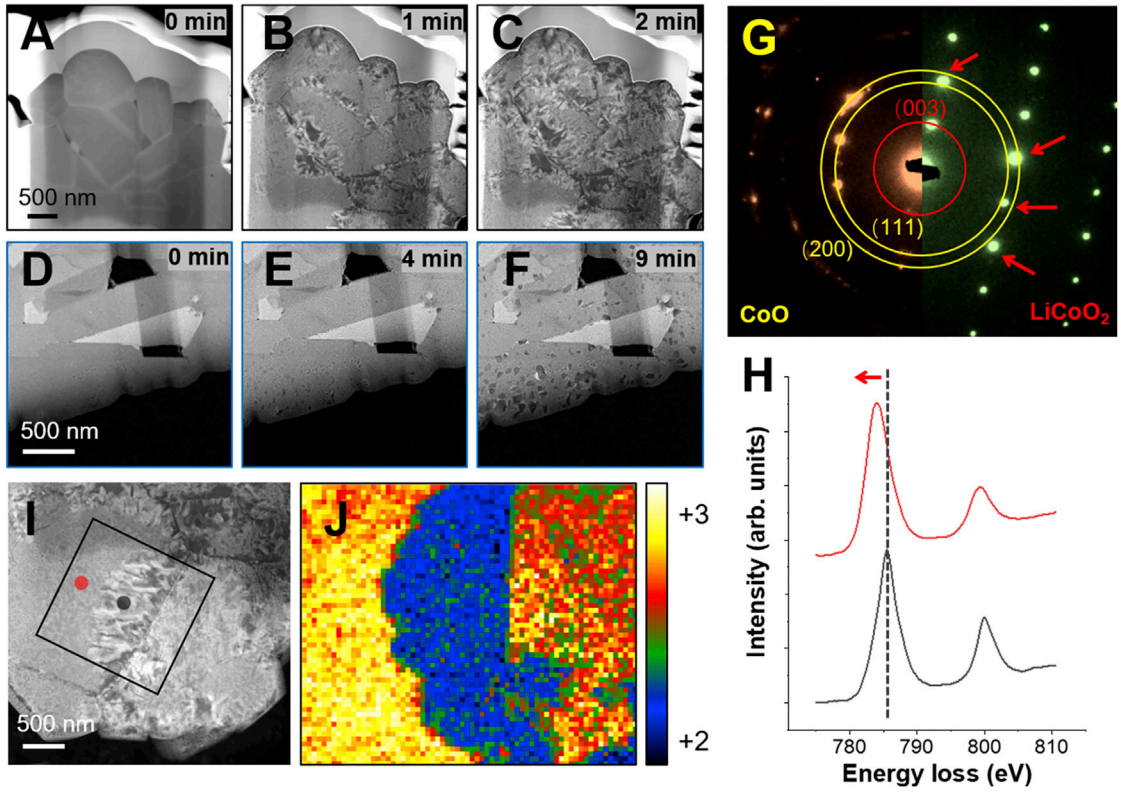

Figure 1. Heterogeneity of the induced boundary oxygen release by changing the heating rate

(A–C) Thermal behavior of the LCO cathode under a high heating rate. It shows a boundary-driven degradation with an interface to interior propagation.

(D–F) Thermal behavior of the LCO cathode under a low heating rate. The degradation is through the growth of surface nanovoids, which is insensitive to the appearance of the intergranular boundaries.

(G) Zone axis electron diffraction along the [100] direction of the pristine LCO in front of and behind a reaction front, indicated by the red and black dots in (I).

(H) The corresponding Co L edges in front of and behind the reaction front indicated by the same red and black dots in (I).

(I) Propagation of the oxygen release degradation initiated at an intergranular boundary. It shows a strong anisotropy pathway, in which the reaction front moves toward 1 grain while the other grain is almost intact.

(J) Covalence state map of the black rectangular area in (I).

a robust behavior difference indicates an underlying physics originating from the intrinsic structure property of layered cathodes.

Figure 1G is the electron diffraction pattern selected from areas in front of and behind the reaction front, indicated by red and black dots in Figure 1I. It shows a clear layered-to-rock salt (RS) phase transition as the reaction front propagates. Electron energy loss spectroscopy (EELS) also confirms the reduction of Co, as can be deduced from the clear shift of the Co L_3 edges in Figure 1H. The diffraction spots of the RS phase show a strong crystal orientation relationship to the spots of the layered phase (red arrows), which indicates a topotactic phase transition even under significant phase degradation. The quantification of the Co valence is estimated from a linear interpolation based on the amount of the Co L_3 shift, with the Co valence state map plotted in Figure 1J. It reveals a sharp reduction front of Co which also indicates an abrupt release of oxygen following the same boundary-to-interior pathway. This is significantly different from the oxygen release at slow heating rates, which generally follows the stepwise layered to spinel and RS phase transitions, and almost evenly disperses on the surface as nanovoids (Figures 1D–1F).[20,30,32] No gradient of the Co valence states can be observed with the propagating of the

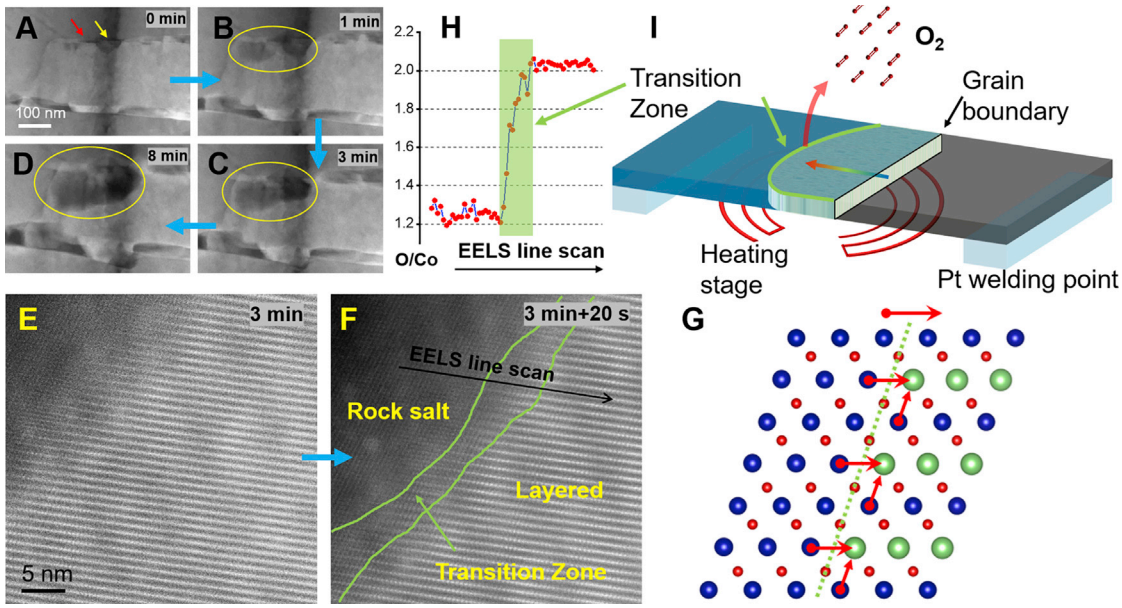

Figure 2. Propagation of the boundary-driven oxygen release degradation

(A–D) Dynamic tracking of the degradation propagation from a mismatch intergranular boundary with a strong thickness variation. The reaction initiates at the thin area of the boundary; the propagation does not follow the thin area but rather adapts a clear crystallographic orientation.

(E and F) HAADF STEM images showing the migration of the reaction front toward the layered direction. The reaction front can be viewed as a narrow transition zone between the rock salt and layered phase.

(G) Corresponding atomic model of the reaction front.

(H) The O:Co ratio from the EELS line scan along the black arrow in (F).

(I) Schematic illustration of the chip-based *in situ* heating experiment.

reaction front (Figure 1J). It indicates that the lattice oxygen is abruptly released on the reaction front, rather than progressively averaged on the surface, which presents a much more severe issue than that of bulk degradation.

Surface effect and crystal orientation dependence on inward propagation of oxygen loss

As most thermal runway accidents always involve an abrupt temperature increase, the inward oxygen release propagation is a critical concern for battery safety and performance. Understanding the driving force for the inward degradation is crucial. Figure 2A is a LCO secondary particle mounted on the chip-based heating stage. A high-mismatch boundary with a sharp edge is selected for observation (red arrow). A ~70-nm boundary area (yellow arrow in Figure 2A) having a thinner sample thickness is created by the curtaining effect of the ion beam milling; it is viewed as a dark contrast stripe because of the mass sensitive effect of the HAADF signal.[30] The sample is heated to 550°C at a fast heating rate to initiate the boundary reaction and then remains at a slightly lower temperature (500°C) to slow down the inward propagation and to allow direct imaging of the degrading dynamics. As shown in Figures 2A–2D, oxygen release starts at the thin area of the mismatched boundary and preferably propagates through one grain, while the grain on the other side of the boundary remains almost intact. Figures 2E and 2F are HAADF STEM images of the reaction front. It shows a clear layered/RS interface (atomic model in Figure 2G), which agrees with the electron diffraction in Figure 1G. A narrow transition zone of 2–6 nm between the layered and RS phases can be observed in Figure 2F, which indicates a fast oxygen loss as the reaction front propagates. This is also supported by the abrupt O:Co ratio change from the EELS line scan (green area in Figure 2H).

For the chip-based stage, the curtaining region (dark strip in Figure 2A) has a thinner thickness and a larger surface:bulk ratio. It will facilitate reactions that rely on short-range cation migration, since the surface provides a fast migration path with higher reaction kinetics.[7,30,32] However, the migration of oxygen vacancies is relatively easier, but the activation energy is still as high as 1.5 eV. Oxygen diffusion can be facilitated by high-voltage cycling or high-temperature conditions,[30,32] which increase the migration length and introduces a strong crystallographic anisotropy. With the start of the oxygen loss on the boundary, a gradient of the lattice oxygen content is established that keeps injecting oxygen vacancies into the neighboring bulk interiors.[32] Oxygen vacancies break the kinetic stability by compromising the metal-oxygen octahedra trapping strength,[7] which results in a boundary-to-interior degradation propagating through the favorable diffusion path of the oxygen vacancies. This is the reason that the degradation shows a strong crystallographic orientation dependence and does not follow the high surface ratio areas (dark strip) once initiated on the boundary. As a result, the degradation is induced along the intergranular interface, but the grain with an unfavorable oxygen diffusion pathway remains intact. Such an effect can also be observed in Figure 1I; the whole right-side grain is almost insensitive to oxygen loss. A schematic illustration of the favorable crystallographic orientation propagation effect is shown in Figure 2I.

Increased oxygen loss susceptibility from the interfacial planar gliding

Normally, the thermal-driven oxygen release is strongly dependent on the highest temperature, to which most previous reports also refer as the threshold or onset temperature for the oxygen release, while generally ignoring the effect of the heating history. Oxygen release susceptibility is also assumed to be area independent. Our results indicate that both parameters are much more elusive. To understand the mechanism of the boundary-driven effect, HAADF STEM imaging with a short pixel dwell time of 10 μs was used to capture the boundary structure that initiates the degrading. Figures 3A and 3B show the boundary structure before and right at the degrading, respectively. A clear planar gliding can be observed (yellow lines and red dots) with an additional contrast in the Li layer (green arrows), which reveals Co cross-layer migration that indicates the onset of the oxygen release degradation.[2,3,7,32] Density functional theory (DFT) calculations are performed to understand the gliding and stress effect on the boundary degradation. The shear stress is introduced by applying an in-plane planar gliding according to the STEM images. With the lattice relaxation that accommodates the shear stress, an obvious distortion of the CoO_6 octahedra can be observed, as indicated by the red arrow on the right side of Figure 3B. This also agrees with the STEM image where the gliding area shows a diffuse contrast. The metal-oxygen octahedra framework plays a significant role in the kinetic stability of LCO cathodes. Co ions are always kinetically trapped inside the CoO_6 octahedra bonding network, in which the structure integrity is maintained even when the thermodynamic driving force for a phase transition largely exists.[40] Slight structure modifications of the CoO_6 octahedra were actually reported to have a significant effect on its stability.[7,32] To quantify the kinetic stability, the cross-layer migration barrier is calculated using the climbing image-nudged elastic band (CI-NEB) method, following the same approach used in our previous work (calculation details can be found in the supplemental information).[7,32] Figure 3C is the Co migration barrier as a function of the planar gliding ratio along the [100] direction. The migration barrier drops from 2.33 eV to a minimum of 0.96 eV in the presence of a planar gliding, which reveals a highly reduced boundary kinetic stability by compromising the trapping strength of the CoO_6 framework. Different gliding vectors are considered, which also results in a reduced stability regardless of the gliding direction. A large quantitative variation of the stability reduction is also

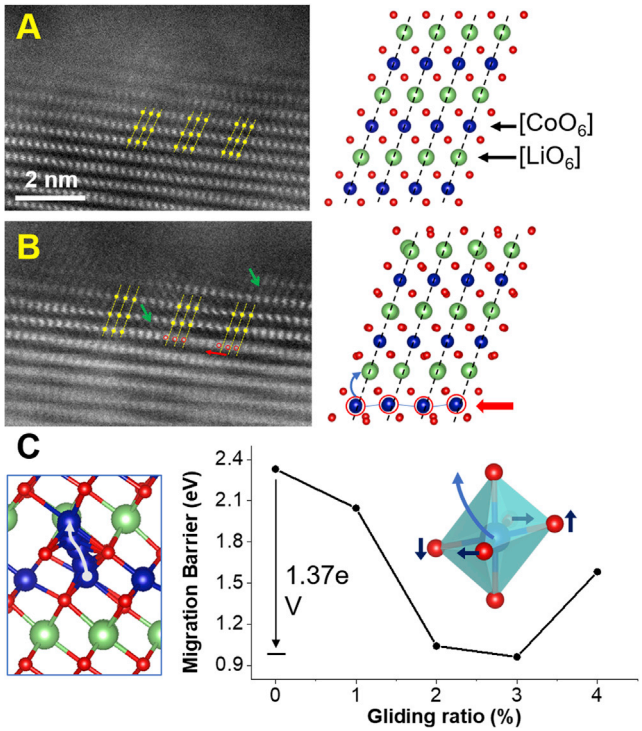

Figure 3. Density functional calculation of the planar gliding-driven phase degradation

(A and B) HAADF STEM images of an intergranular boundary before and right at the degradation. The corresponding atomic model is shown on the right side of the STEM images. A clear planar gliding can be viewed when the phase degradation is just initiated (Co cross-layer migration as indicated by the blue arrows).

(C) The Co cross-layer migration barrier as a function of the planar gliding ratio (the planar gliding distance to the lattice parameter) calculated by the climbing image-nudged elastic band method.

revealed, and the structure is much more vulnerable by gliding perpendicular to the edges of the CoO_6 octahedra (Figure S3 and Note S3).

It is interesting that the migration barrier does not decrease linearly with the increasing strength of the planar gliding. The barrier reaches the minimum at a gliding ratio of 1%–3% (Figure S3), which means that the structure is most vulnerable when the gliding has just initiated. This is likely to be a more complicated reconstruction of the local CoO_6 units and neighboring structures that makes Co difficult to diffuse through the original interstitial sites with increasing gliding and stress. Although the planar gliding in the layered cathodes has been recognized and its reversible feature has also been reported recently,[41] a quantitative structure dynamic in the gliding process is still far from clear, as a quasi-static reconstruction at large gliding ratios has not been proved yet. Further investigation into a dynamic structure-gliding correlation is still needed.

Since the kinetic stability is sensitive to both the gliding ratio and the direction, a junction point with multiple interfaces is more likely to generate an interfacial condition that favors the oxygen release. Figure 4 is a LCO secondary particle that undergoes a similar high heating rate experiment. Various intergranular boundaries with multiple interface connections are present. As expected, oxygen release is initiated at the interface triple point, which indicates that the oxygen release susceptibility is not only materials dependent but also a function of the local situation. Due to

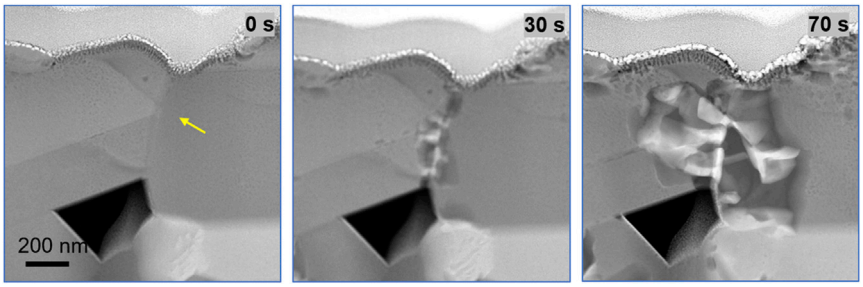

Figure 4. Dynamic tracking of a LCO cathode with multiple intergranular interfaces at high heating rate

Increased oxygen release susceptibility at multiple interface junctions.

the diffusion of oxygen vacancies that continuously breaks the kinetic stability of the layered structure, once the degradation is initiated, the oxygen release has a strong propagating effect that keeps degrading the neighboring areas. This means that the threshold for degradation depends on the area that is most vulnerable. Materials design for stable cathodes should focus on eliminating the most unstable structures, which include high-mismatch interfaces, surface, multiple junctions, as well as planar gliding and antiphase defects.[42].

Fast-degrading dynamics-induced interface nano cracking

The layered/RS interface is able to maintain a relatively slow degrading dynamics, as can be seen in both Figures 1 and 2, which shows a stable migration of the layered/RS interface from the intergranular boundary toward the particle interiors. However, with fast-degrading dynamics, nano cracks can appear by breaking the layered/RS interface at the intergranular boundaries; this is attributed to the weak bonding strength and the strong ion migration dynamics at the interface that makes it mechanically less stable than the bulk.[43] Figures 5A and 5B are HAADF STEM images of a boundary that has undergone multiple heating cycles from room temperature to 550°C at a heating rate of 60°C/s. The dark contrast (yellow arrows) in Figure 5A indicates a strong stress accumulation or cation migration-associated mass loss on the boundary, which turns into nano-sized cracking after several cycles with strong cation dynamics on the boundary (green arrows in Figure 5B). The cracking continues to tear off the boundary and stops at a width of ~2 nm (Figure S4). Most of the cracking generally stops within several nanometers as the stress effect no longer exists and the cation migration ceases once the boundary breaks.

Similar nano-sized cracking at the intergranular interface can also be observed after the very first electrochemical cycling, as shown in Figure 5C. A strong cation cross-layer migration can be observed on the boundary (green arrow) that drives the intergranular cracking (yellow arrows), which also supports the effect of the cation migration on the nano crack formation. It was recently recognized that the thermal stability and electrochemical cycling stability share the same degrading feature on oxygen release,[4] which is also the reason why similar nano cracks are found by either cycling or thermal effect since they find their origin in the intrinsic structure instability of the layered cathodes. This cation migration eventually leads to a transformation into the RS phase that induces an increasing Li transport anisotropy right on the layered/RS interface. This has been recently reported to be at the origin of the (003) layered cracks after extended cycling.[43,44] Our results indicate that cracking can actually occur already at the first cycle due to the cation migration itself, which becomes severe in Ni-rich LTMOs since Ni ions are much easier to migrate. This nano-sized

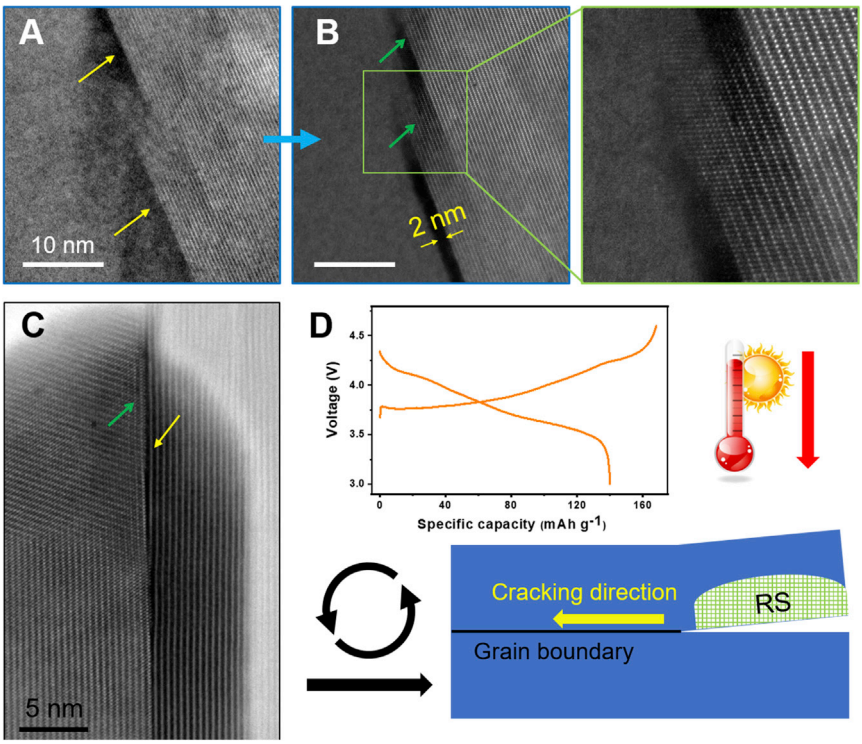

Figure 5. Formation of nano cracks under fast cation migration dynamics

(A and B) Intergranular boundary of a LCO cathode that undergoes multiple fast-heating cycles. It shows a clear stress accumulation (yellow arrows) leading to crack formation (blue arrows). The cracking tip shows a strong cation cross-layer migration (inset of B).

(C) Formation of nano cracks at the intergranular boundaries of NCM 811 after the first electrochemical cycle.

(D) The corresponding first-cycle voltage profile.

intergranular cracking may contribute to the first cycle irreversible capacity loss, which is a common issue for Ni-rich LTMOs (Figure 5D).

It should be noted that the effect of cation cross-layer migration is still under debate. Controversial results were widely reported with respect to the contribution of cation migration to the cathode stability.[44–49] Our results indicate that the dynamics of the migration is also critical. This is significant for most layered cathodes with secondary agglomerates, as the internal strain from the sluggish volume dynamics can be accommodated by slightly adjusting the relative position of the primary particles, while the strain is hard to release with the fast volume change since the adjustment of primary particles is still rigid. However, it has been documented recently that cation cross-layer migration is also reversible, similar to the insertion/extraction of alkali metal ions.[46,49] As a local volume change is also involved, the repetitive growth and decay of the spinel phase from the reversible cation migration would impose a strong internal stress toward crack formation. Due to the strong surface effect (Figure 2), it can be expected that the intergranular cracks tend to initiate at the surface of the secondary particles, and the buried intergranular boundary without direct surface exposure will be more kinetically stable toward anisotropic lattice expansion/contraction. This argument is supported by the recent reported observation that shows that the nano cracks initiate at the surface end of the high-energy phase boundaries.[36] It is also the reason that surface coating at the secondary particle level can significantly suppress the cathode degradation.

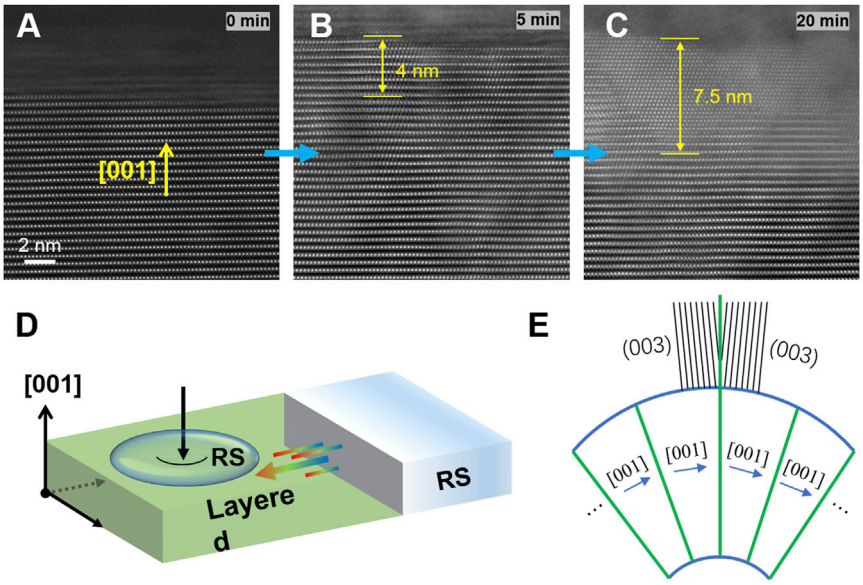

Figure 6. Shielding effect of the planar layers

(A–C) Propagation of the phase degradation across the planar layers. Compared with the through-layer propagation in Figure 2, it shows a much slower degradation diffusion across the planar layers.

(D) Schematic illustration of the anisotropic diffusion pathway of the phase degradation.

(E) Columnar grains with low-angle boundaries are proposed to obtain a high-boundary oxygen stability.

Columnar grains with low-angle boundaries toward stronger-boundary oxygen stability

Single-crystal cathodes have been proposed to avoid secondary boundaries; this would completely remove the interface effect.[50] However, single-crystal cathodes still undergo a reversible gliding process during charging and discharging.[41] Recognition of the shear stress and the effect of planar gliding on the structure degradation is essential for cathode design. Avoiding the shear stress by radially orienting the primary particles with the planar layered interfaces would be the ideal way to minimize boundary stress-induced degradation. A layered interface can also shield the propagation of oxygen release and degradation by preventing the vacancy and ion migration, as shown in Figures 6A–6C. It is the same fast heating experiment, but it shows a very slow degradation across the planar layers. The growth of the RS phase almost ceases at ~7.5 nm along the [001] direction without further penetrating into the bulk (Figure 6C). A schematic illustration of the layered shielding effect is shown in Figure 6D. The corresponding cathode design is shown in Figure 6E, in which the presence of multiple columnar grains with low-angle planar boundaries is proposed to reduce the boundary effect, as well as the propagation of any potential degradation toward the grain interior. The columnar design was also recently found to achieve a long-term cycling stability.[48] It should be noted, however, that due to the spherical shape of the cathodes, the density of the radially patterned low-angle boundaries will quickly increase toward the core area, which becomes unfavorable and will lead to highly mismatched boundaries. However, without direct exposure to the electrolyte, a buried cracking close to the center of the cathode has less effect on the performance decay.

Finally, it has been reported that the extended lithiation/delithiation process introduces a strong anisotropic contraction/expansion that leads to stress accumulation

among primary particles and promotes crack formation in the secondary particles.[51] Although it is worth noting that aberration may exist by directly comparing this result to other layered systems, our fast-heating experiment provides a similar strain effect from a thermal approach,[36,37,41] which is highly illustrative for predicting the cracking behavior without going through a long cycling process. In addition, the electrochemical cycling (especially at high voltage) will introduce a continuous surface oxygen release, and the oxygen release stress also plays a critical role in the detachment of the primary particles.[10] A fast-heating experiment in vacuum also accelerates the oxygen loss by reducing the chemical potential of oxygen, which serves as a strong indicator of crack formation analog to the electrochemical cycling.

Chip-based *in situ* STEM heating experiments were performed. Dynamic atomic-level imaging of the boundary oxygen release driven by the planar gliding has been obtained. The imaging reveals a strong inward diffusion to the bulk interior through a layered pathway with abrupt oxygen losses right at the narrow propagation front. The gliding induces a complicated distortion of the metal-oxygen octahedra framework and significantly reduces the cation migration barrier, which is highly correlated with the initiation of the oxygen release. Since most of the secondary boundaries in an actual working cathode are kinetically formed at high mismatch states, the local stress anisotropy is always significantly accumulated on the boundary during the electrochemical cycling. This could lead to planar gliding as an intrinsic structure instability in layered cathodes. Our results provide an atomic insight into the boundary oxygen release degradation, and they indicate that radially patterned columnar grains with low-angle planar boundaries are an efficient mitigating approach to reduce the initiation of the boundary degradation as well as the inward propagation.

EXPERIMENTAL PROCEDURES

Resource availability

Lead contact

Further information and requests for resources and reagents can be directed to the lead contact, Prof. Jinsong Wu (wujs@whut.edu.cn).

Materials availability

This study did not generate new unique reagents.

Data and code availability

The authors declare that the data supporting the findings of this study are available within the article and the supplemental information. All other data are available from the lead contact upon reasonable request.

Preparation of samples and *in situ* experiments

In situ STEM samples were prepared by a FEI Helios Nanolab G3 dual-beam focused ion beam (FIB) using a standard lift-out procedure following our previous report.[7,52] The sample was pre-coated by carbon films and then deposited with e-beam-induced carbon/Pt deposition inside the FIB chamber. The sample was transferred onto a *DENSsolution* heating chip, with the target area polished multiple times to a specific TEM sample thickness. The SiN_x chip-supporting film was milled for better imaging conditions. The prepared heating chip was directly loaded into the microscope for the *in situ* experiment right after sample preparation. The detailed *in situ* stage setting can be found in our previous report.[7]

Microstructure characterizations

The STEM images and EELS spectra were performed in an CEOS probe-corrected FEI Themis TEM at an electron accelerating voltage of 300 kV, with a probe convergence angle of 17.8 mrad, spatial resolution of 0.08 nm, and probe current of ~30 pA for STEM imaging and ~100 pA for EELS acquisition. The inner semiangular angle for the HAADF detector is 84 mrad for STEM imaging. EELS was performed using the Gatan Quantum 965 GIF system. Dual EELS was taken with a spectrometer dispersion chosen for simultaneous visualization of zero loss, O, K, and Co L edges. The energy resolution determined by full-width at half-maximum of the zero-loss peak was ~1.3 eV. The background was subtracted using the power law method, with plural scattering removed by Fourier-ratio deconvolution.

Calculation method

Ab initio calculations were performed using the VASP (Vienna Ab-initio Simulation Package). Perdew-Burke-Ernzerhof (PBE) generalized gradient approximation (GGA) was selected for the electronic exchange-correlation function. The GGA + U method was used to correct the strong electronic correlation among the localized Co 3d electrons with coulomb repulsion U = 3.91 eV. The energy cutoff for the plane-wave basis expansion was chosen at 520 eV. An energy difference of 1.0×10^{-5} eV/atom was set to obtain the accurate electronic ground-state calculation. The maximum force tolerance was set to 0.02 eV/Å for structural optimization. The k-points for the Brillouin zone were selected by the Monkhorts-Pack method and set to 4 × 4 × 2. The CI-NEB method was carried out for the diffusion simulation of the Co atom in $LiCoO_2$ systems with a different strength of the planar gliding, with 4 climbing images between initial and final states generated through the transition state tools for VASP (VASP + VTST).

Electrochemistry test

The commercially available $LiCoO_2$ (LCO) and $LiNi_{0.8}Co_{0.1}Mn_{0.1}O_2$ (NCM811) cathode were used for this study. As this work is based on a direct comparison of the boundary and its neighboring area, the pristine LCO sample is used to rule out the state of charge inhomogeneity across the boundary. As a result, the observed different behaviors between the boundary and its neighboring regions can be attributed to the intrinsic structure property. The NCM811 was electrochemically cycled in the voltage range of 3.0–4.6 V (versus Li^+/Li) at 100 mA g^{-1}. The coin cell is assembled with Li-metal foil as the anode in a glovebox filled with pure Ar gas. The cathode electrodes were composed of 80% active material (NCM811), 10% acetylene black, and 10% polyvinylidene fluoride (PVDF), which were mixed and the resulting slurry was coated onto Al foil. A solution of ethylene carbonate (EC), diethyl carbonate (DEC), and dimethyl carbonate (DMC) (1:1:1 ratio/volume) was used as the electrolyte. It is worth noting that under such conditions, the performance of the commercial NCM811 is not comparable to the lab-optimized counterpart, but it represents the general issue in a practical service condition. A quantitative comparison may be altered based on the different performance and service conditions. The coin cells were disassembled after the first cycle and at the discharge state. The cathode material was immersed in a pure DMC solution before loading onto a polished Cu stage.

SUPPLEMENTAL INFORMATION

Supplemental information can be found online at https://doi.org/10.1016/j.xcrp.2021.100695.

ACKNOWLEDGMENTS

This work was supported by the National Natural Science Foundation of China (22005230 and 52072282). The S/TEM work was performed at the Nanostructure Research Center (NRC), which is supported by the Fundamental Research Funds for the Central Universities (WUT: 2021III016GX).

AUTHOR CONTRIBUTIONS

C.S., Y.Z., and J.W. conceived the project. C.S., H.P., and J.W. performed the *in situ* TEM and interpretation. X.L. and Y.Z. conducted the DFT simulations. H.P. conducted the battery measurement and data interpretation. All of the authors contributed to the writing of the manuscript before submission.

DECLARATION OF INTERESTS

The authors declare no competing interests.

Received: August 20, 2021
Revised: October 7, 2021
Accepted: November 25, 2021
Published: December 20, 2021

REFERENCES

1. Sharifi-Asl, S., Lu, J., Amine, K., and Shahbazian-Yassar, R. (2019). Oxygen Release Degradation in Li-Ion Battery Cathode Materials: Mechanisms and Mitigating Approaches. Adv. Energy Mater. *9*, 1900551.

2. Chen, J., Deng, W., Gao, X., Yin, S., Yang, L., Liu, H., Zou, G., Hou, H., and Ji, X. (2021). Demystifying the Lattice Oxygen Redox in Layered Oxide Cathode Materials of Lithium-Ion Batteries. ACS Nano *15*, 6061–6104.

3. Sathiya, M., Abakumov, A.M., Foix, D., Rousse, G., Ramesha, K., Saubanère, M., Doublet, M.L., Vezin, H., Laisa, C.P., Prakash, A.S., et al. (2015). Origin of voltage decay in high-capacity layered oxide electrodes. Nat. Mater. *14*, 230–238.

4. Hu, E., Yu, X., Lin, R., Bi, X., Lu, J., Bak, S., Nam, K.-W., Xin, H.L., Jaye, C., Fischer, D.A., et al. (2018). Evolution of redox couples in Li- and Mn-rich cathode materials and mitigation of voltage fade by reducing oxygen release. Nat. Energy *3*, 690–698.

5. Liu, H., Wolf, M., Karki, K., Yu, Y.-S., Stach, E.A., Cabana, J., Chapman, K.W., and Chupas, P.J. (2017). Intergranular Cracking as a Major Cause of Long-Term Capacity Fading of Layered Cathodes. Nano Lett. *17*, 3452–3457.

6. Chen, J., Zou, G., Deng, W., Huang, Z., Gao, X., Liu, C., Yin, S., Liu, H., Deng, X., Tian, Y., et al. (2020). Pseudo-Bonding and Electric-Field Harmony for Li-Rich Mn-Based Oxide Cathode. Adv. Funct. Mater. *30*, 2004302.

7. Sun, C., Liao, X., Xia, F., Zhao, Y., Zhang, L., Mu, S., Shi, S., Li, Y., Peng, H., Van Tendeloo, G., et al. (2020). High-Voltage Cycling Induced Thermal Vulnerability in $LiCoO_2$ Cathode: Cation Loss and Oxygen Release Driven by Oxygen Vacancy Migration. ACS Nano *14*, 6181–6190.

8. Seong, W.M., Yoon, K., Lee, M.H., Jung, S.-K., and Kang, K. (2019). Unveiling the Intrinsic Cycle Reversibility of a $LiCoO_2$ Electrode at 4.8-V Cutoff Voltage through Subtractive Surface Modification for Lithium-Ion Batteries. Nano Lett. *19*, 29–37.

9. Wu, F., Tian, J., Liu, N., Lu, Y., Su, Y., Wang, J., Chen, R., Ma, X., Bao, L., and Chen, S. (2017). Alleviating structural degradation of nickel-rich cathode material by eliminating the surface Fm3m phase. Energy Storage Mater. *8*, 134–140.

10. Mu, L., Lin, R., Xu, R., Han, L., Xia, S., Sokaras, D., Steiner, J.D., Weng, T.-C., Nordlund, D., Doeff, M.M., et al. (2018). Oxygen Release Induced Chemomechanical Breakdown of Layered Cathode Materials. Nano Lett. *18*, 3241–3249.

11. Nadimpalli, S., and Abraham, D. (2015). Stress Evolution in Lithium-Ion Composite Electrodes during Electrochemical Cycling and Resulting Internal Pressures on the Cell Casing. J. Electrochem. Soc. *162*, A2656.

12. Miller, D.J., Proff, C., Wen, J.G., Abraham, D.P., and Bareño, J. (2013). Observation of Microstructural Evolution in Li Battery Cathode Oxide Particles by In Situ Electron Microscopy. Adv. Energy Mater. *3*, 1098–1103.

13. Lee, E.-J., Chen, Z., Noh, H.-J., Nam, S.C., Kang, S., Kim, D.H., Amine, K., and Sun, Y.-K. (2014). Development of microstrain in aged lithium transition metal oxides. Nano Lett. *14*, 4873–4880.

14. Mukhopadhyay, A., and Sheldon, B.W. (2014). Deformation and stress in electrode materials for Li-ion batteries. Prog. Mater. Sci. *63*, 58–116.

15. Kızıltaş-Yavuz, N., Herklotz, M., Hashem, A.M., Abuzeid, H.M., Schwarz, B., Ehrenberg, H., Mauger, A., and Julien, C.M. (2013). Synthesis, structural, magnetic and electrochemical properties of $LiNi_{1/3}Mn_{1/3}Co_{1/3}O_2$ prepared by a sol–gel method using table sugar as chelating agent. Electrochim. Acta *113*, 313–321.

16. Robert, R., and Novák, P. (2015). Structural Changes and Microstrain Generated on $LiNi_{0.80}Co_{0.15}Al_{0.05}O_2$during Cycling: Effects on the Electrochemical Performance. J. Electrochem. Soc. *162*, A1823–A1828.

17. Hwang, S., Kim, S.M., Bak, S.-M., Kim, S.Y., Cho, B.-W., Chung, K.Y., Lee, J.Y., Stach, E.A., and Chang, W. (2015). Using Real-Time Electron Microscopy To Explore the Effects of Transition-Metal Composition on the Local Thermal Stability in Charged $Li_xNi_yMn_zCo_{1-y-z}O2$ Cathode Materials. Chem. Mater. *27*, 3927–3935.

18. Karki, K., Huang, Y., Hwang, S., Gamalski, A.D., Whittingham, M.S., Zhou, G., and Stach, E.A. (2016). Tuning the Activity of Oxygen in $LiNi_{0.8}Co_{0.15}Al_{0.05}O_2$ Battery Electrodes. ACS Appl. Mater. Interfaces *8*, 27762–27771.

19. Sharifi-Asl, S., Soto, F.A., Foroozan, T., Asadi, M., Yuan, Y., Deivanayagam, R., Rojaee, R., Song, B., Bi, X., Amine, K., et al. (2019). Anti-Oxygen Leaking LiCoO2. Adv. Funct. Mater. *29*, 1901110.

20. Sharifi-Asl, S., Soto, F.A., Nie, A., Yuan, Y., Asayesh-Ardakani, H., Foroozan, T., Yurkiv, V., Song, B., Mashayek, F., Klie, R.F., et al. (2017). Facet-Dependent Thermal Instability in $LiCoO_2$. Nano Lett. *17*, 2165–2171.

21. Hwang, S., Lee, Y., Jo, E., Chung, K.Y., Choi, W., Kim, S.M., and Chang, W. (2017). Investigation of Thermal Stability of P2-Na_xCoO_2 Cathode Materials for Sodium Ion Batteries Using Real-Time Electron Microscopy. ACS Appl. Mater. Interfaces *9*, 18883–18888.

22. Bak, S.M., Hu, E., Zhou, Y., Yu, X., Senanayake, S.D., Cho, S.J., Kim, K.B., Chung, K.Y., Yang, X.Q., and Nam, K.W. (2014). Structural changes and thermal stability of charged LiNixMnyCozO2 cathode materials studied by combined in situ time-resolved XRD and mass spectroscopy. ACS Appl. Mater. Interfaces *6*, 22594–22601.

23. McCalla, E., Abakumov, A.M., Saubanère, M., Foix, D., Berg, E.J., Rousse, G., Doublet, M.-L., Gonbeau, D., Novák, P., Van Tendeloo, G., et al. (2015). Visualization of O-O peroxo-like dimers in high-capacity layered oxides for Li-ion batteries. Science *350*, 1516–1521.

24. Liu, T., Lin, L., Bi, X., Tian, L., Yang, K., Liu, J., Li, M., Chen, Z., Lu, J., Amine, K., et al. (2019). In situ quantification of interphasial chemistry in Li-ion battery. Nat. Nanotechnol. *14*, 50–56.

25. Yoon, W.-S., Balasubramanian, M., Yang, X.-Q., McBreen, J., and Hanson, J. (2005). Time-Resolved XRD Study on the Thermal Decomposition of $Li_{1-x}Ni_{0.8}Co_{0.15}Al_{0.05}O_2$ Cathode Materials for Li-Ion Batteries. Electrochem. Solid-State Lett. *8*, A83–A86.

26. Belharouak, I., Lu, W., Liu, J., Vissers, D., and Amine, K. (2007). Thermal behavior of delithiated $Li(Ni_{0.8}Co_{0.15}Al_{0.05})O_2$ and $Li1.1(Ni_{1/3}Co_{1/3}Mn_{1/3})_{0.9}O_2$ powders. J. Power Sources *174*, 905–909.

27. Wu, L., Nam, K.-W., Wang, X., Zhou, Y., Zheng, J.-C., Yang, X.-Q., and Zhu, Y. (2011). Structural Origin of Overcharge-Induced Thermal Instability of Ni-Containing Layered-Cathodes for High-Energy-Density Lithium Batteries. Chem. Mater. *23*, 39533960.

28. Tan, H., Takeuchi, S., Bharathi, K.K., Takeuchi, I., and Bendersky, L.A. (2016). Microscopy Study of Structural Evolution in Epitaxial $LiCoO_2$ Positive Electrode Films during Electrochemical Cycling. ACS Appl. Mater. Interfaces *8*, 6727–6735.

29. Ben, L., Yu, H., Chen, B., Chen, Y., Gong, Y., Yang, X., Gu, L., and Huang, X. (2017). Unusual Spinel-to-Layered Transformation in $LiMn_2O_4$ Cathode Explained by Electrochemical and Thermal Stability Investigation. ACS Appl. Mater. Interfaces *9*, 35463–35475.

30. Yan, P., Zheng, J., Tang, Z.K., Devaraj, A., Chen, G., Amine, K., Zhang, J.G., Liu, L.M., and Wang, C. (2019). Injection of oxygen vacancies in the bulk lattice of layered cathodes. Nat. Nanotechnol. *14*, 602–608.

31. Bak, S.-M., Nam, K.-W., Chang, W., Yu, X., Hu, E., Hwang, S., Stach, E.A., Kim, K.-B., Chung, K.Y., and Yang, X.-Q. (2013). Correlating Structural Changes and Gas Evolution during the Thermal Decomposition of Charged $Li_xNi_{0.8}Co_{0.15}Al_{0.05}O_2$ Cathode Materials. Chem. Mater. *25*, 337–351.

32. Li, C.-F., Zhao, K., Liao, X., Hu, Z.-Y., Zhang, L., Zhao, Y., Mu, S., Li, Y., Li, Y., Van Tendeloo, G., et al. (2021). Interface cation migration kinetics induced oxygen release heterogeneity in layered lithium cathodes. Energy Storage Mater. *36*, 115–122.

33. Liu, X., Xu, G.-L., Yin, L., Hwang, I., Li, Y., Lu, L., Xu, W., Zhang, X., Chen, Y., Ren, Y., et al. (2020). Probing the Thermal-Driven Structural and Chemical Degradation of Ni-Rich Layered Cathodes by Co/Mn Exchange. J. Am. Chem. Soc. *142*, 19745–19753.

34. Lee, J., Papp, J.K., Clément, R.J., Sallis, S., Kwon, D.-H., Shi, T., Yang, W., McCloskey, B.D., and Ceder, G. (2017). Mitigating oxygen loss to improve the cycling performance of high capacity cation-disordered cathode materials. Nat. Commun. *8*, 981.

35. House, R.A., Maitra, U., Jin, L., Lozano, J.G., Somerville, J.W., Rees, N.H., Naylor, A.J., Duda, L.C., Massel, F., Chadwick, A.V., et al. (2019). What Triggers Oxygen Loss in Oxygen Redox Cathode Materials? Chem. Mater. *31*, 3293–3300.

36. Sharifi-Asl, S., Yurkiv, V., Gutierrez, A., Cheng, M., Balasubramanian, M., Mashayek, F., Croy, J., and Shahbazian-Yassar, R. (2020). Revealing Grain-Boundary-Induced Degradation Mechanisms in Li-Rich Cathode Materials. Nano Lett. *20*, 1208–1217.

37. Jiang, Y., Yan, P., Yu, M., Li, J., Jiao, H., Zhou, B., and Sui, M. (2020). Atomistic mechanism of cracking degradation at twin boundary of $LiCoO_2$. Nano Energy *78*, 105364.

38. Yamakawa, S., Yamasaki, H., Koyama, T., and Asahi, R. (2013). Numerical study of Li diffusion in polycrystalline LiCoO2. J. Power Sources *223*, 199–205.

39. Moriwake, H., Kuwabara, A., Fisher, C.A.J., Huang, R., Hitosugi, T., Ikuhara, Y.H., Oki, H., and Ikuhara, Y. (2013). First-principles calculations of lithium-ion migration at a coherent grain boundary in a cathode material, LiCoO(2). Adv. Mater. *25*, 618–622.

40. Wang, L., Maxisch, T., and Ceder, G. (2007). A First-Principles Approach to Studying the Thermal Stability of Oxide Cathode Materials. Chem. Mater. *19*, 543–552.

41. Bi, Y., Tao, J., Wu, Y., Li, L., Xu, Y., Hu, E., Wu, B., Hu, J., Wang, C., Zhang, J.-G., et al. (2020). Reversible planar gliding and microcracking in a single-crystalline Ni-rich cathode. Science *370*, 1313–1317.

42. Li, S., Yao, Z., Zheng, J., Fu, M., Cen, J., Hwang, S., Jin, H., Orlov, A., Gu, L., Wang, S., et al. (2020). Direct Observation of Defect-Aided Structural Evolution in a Nickel-Rich Layered Cathode. Angew. Chem. Int. Ed. Engl. *59*, 22092–22099.

43. Zhang, H., Omenya, F., Yan, P., Luo, L., Whittingham, M.S., Wang, C., and Zhou, G. (2017). Rock-Salt Growth-Induced (003) Cracking in a Layered Positive Electrode for Li-Ion Batteries. ACS Energy Lett. *2*, 2607–2615.

44. Lin, Q., Guan, W., Zhou, J., Meng, J., Huang, W., Chen, T., Gao, Q., Wei, X., Zeng, Y., Li, J., et al. (2020). Ni-Li anti-site defect induced intragranular cracking in Ni-rich layer-structured cathode. Nano Energy *76*, 105021.

45. Su, Y., Yang, Y., Chen, L., Lu, Y., Bao, L., Chen, G., Yang, Z., Zhang, Q., Wang, J., Chen, R., et al. (2018). Improving the cycling stability of Ni-rich cathode materials by fabricating surface rock salt phase. Electrochim. Acta *292*, 217–226.

46. Eum, D., Kim, B., Kim, S.J., Park, H., Wu, J., Cho, S.-P., Yoon, G., Lee, M.H., Jung, S.-K., Yang, W., et al. (2020). Voltage decay and redox asymmetry mitigation by reversible cation migration in lithium-rich layered oxide electrodes. Nat. Mater. *19*, 419–427.

47. Guo, S., Sun, Y., Liu, P., Yi, J., He, P., Zhang, X., Zhu, Y., Senga, R., Suenaga, K., Chen, M., et al. (2018). Cation-mixing stabilized layered oxide cathodes for sodium-ion batteries. Sci. Bull. (Beijing) *63*, 376–384.

48. Kim, U.-H., Park, G.-T., Son, B.-K., Nam, G.W., Liu, J., Kuo, L.-Y., Kaghazchi, P., Yoon, C.S., and Sun, Y.-K. (2020). Heuristic solution for achieving long-term cycle stability for Ni-rich layered cathodes at full depth of discharge. Nat. Energy *5*, 860–869.

49. Zhang, X., Guo, S., Liu, P., Li, Q., Xu, S., Liu, Y., Jiang, K., He, P., Chen, M., Wang, P., et al. (2019). Capturing Reversible Cation Migration in Layered Structure Materials for Na-Ion Batteries. Adv. Energy Mater. *9*, 1900189.

50. Cha, H., Kim, J., Lee, H., Kim, N., Hwang, J., Sung, J., Yoon, M., Kim, K., and Cho, J. (2020). Boosting Reaction Homogeneity in High-Energy Lithium-Ion Battery Cathode Materials. Adv. Mater. *32*, e2003040.

51. Romano Brandt, L., Marie, J.-J., Moxham, T., Förstermann, D.P., Salvati, E., Besnard, C., Papadaki, C., Wang, Z., Bruce, P.G., and Korsunsky, A.M. (2020). Synchrotron X-ray quantitative evaluation of transient deformation and damage phenomena in a single nickel-rich cathode particle. Energy Environ. Sci. *13*, 3556–3566.

52. Sun, C., Zhao, K., He, Y., Zheng, J., Xu, W., Zhang, C., Wang, X., Guo, M., Mai, L., Wang, C., and Gu, M. (2019). Interconnected Vertically Stacked 2D-MoS_2 for Ultrastable Cycling of Rechargeable Li-Ion Battery. ACS Appl. Mater. Interfaces *11*, 20762–20769.